Supporting Information

The electronic state of the His/Tyr–ligated heme of BthA by Mössbauer and DFT analysis.

Andrew Weitz, Saborni Biswas, Kim Rizzolo, Sean Elliott, Emile L. Bominaar, Michael P. Hendrich*

* hendrich@andrew.cmu.edu
Carnegie Mellon University, Dept. of Chemistry, Pittsburgh, PA 15213

S.1 Methods and Materials

S.1.1 Expression and purification of ^{57}Fe-enriched BthA. All reagents were purchased from Sigma Aldrich, unless otherwise noted. The BthA plasmid was co-transformed with pEC86 containing the cytochrome c maturation genes ccmABCDEFGH[1] into E. coli BL21(DE3) competent cells as previously described.[2] ^{57}Fe enriched BthA was prepared through expression of BthA in minimal media supplemented with ^{57}Fe salts. 5 mL starter cultures in 2x YT were grown overnight at 37 °C, supplemented with 100 µg/mL ampicillin and 35 µg/mL chloramphenicol (GoldBio). The cultures were harvested and resuspended in minimal media, containing, per liter: 2 g $(NH_4)_2SO_4$, 14 g K_2HPO_4, 6 KH_2PO_4, and 1 g sodium citrate, 0.2 g $MgSO_4 \bullet 7H_2O$. For each 1 L of media, glucose was added to a final concentration of 0.4% w/v and 10 mL of trace metal solution consisting of (w/v): 0.6% $MgCl_2$, 0.06% $CaCl_2$, 0.01% $MnCl_2$, 0.02% $ZnCl_2$, 0.004% $CuCl_2$, 0.006% $CoCl_2$ and 0.006% Na_2MoO_4, and 1 mL of $^{57}FeCl_2$ (2 mg/L ^{57}Fe, Cambridge Isotopes). The $^{57}FeCl_2$ stock was prepared fresh by dissolving 2 mg ^{57}Fe powder in 1 mL 6 M HCl. The inoculated cultures were incubated at 37 °C and 220 rpm until OD_{600} = 0.8 was reached. Cells were subsequently cooled at 4 °C for 30 minutes, then induced with 100 µM IPTG (GoldBio) for 17 hours at room temperature and shaking at 150 rpm.

Cells were harvested by centrifugation and flash frozen in liquid nitrogen for future protein purification. The protein purification protocol was identical to that previously described.[2] Briefly, cells were lysed by sonication in 50 mM HEPES buffer (GoldBio), pH 7.8, in 300 mM NaCl, 10% v/v glycerol, and 1 mM PMSF (ThermoFisher). After centrifugation at 18,000 g for 30 minutes, the clarified lysate was diluted with the same buffer as above, but NaCl-free to achieve a final [NaCl] = 150 mM. The solution was loaded onto a SP-sepharose cation-exchange buffer (GE Life Sciences), cleaned using 50 mM HEPES buffer at pH 7.8, containing 150 mM NaCl, then finally eluted with HEPES buffer containing 250 mM NaCl. Purity of the eluted fractions were analyzed by 12% SDS-PAGE (BioRad) before pooling the fractions and concentrating to < 2 mL using a 30 kDa MWCO centrifugal filter (Amicon). The concentrated protein was then loaded onto a S-200 size exclusion column (GE Life Sciences) using a BioRad FPLC system. The eluted fractions from size exclusion were also analyzed by 12.5% SDS-PAGE. The pooled fractions were buffer exchanged into 50 mM HEPES, 100 mM NaCl, 10% glycerol at pH 7.8 (storage buffer) and concentrated using a 30 kDa MWCO centrifugal filter. Protein concentrations were determined by Bradford Assay, and subsequently flash frozen in liquid nitrogen, and stored at –80 °C. A typical purified protein had a purity index A_{405nm}/A_{280nm} > 3. The activity of the protein was assayed using the standard ABTS assay in 50 mM

potassium phosphate, pH 6.5 as previously described. All protein assays had k_{cat} and K_m consistent with the previously reported values.

S.1.2 Sample preparation. A concentrated sample of approx. 1.1 mM ^{57}Fe-enriched BthA was prepared as described above. The sample was loaded into a Mössbauer sample holder and flash frozen in liquid nitrogen. To prepare the bis-Fe^{4+} state, an excess of 100 mM H_2O_2 in storage buffer was diluted by a factor 1/10 into the protein-containing solution to ensure full generation of the bis-Fe^{4+} state. The peroxide was pipetted while carefully stirring the solution to allow full mixing with the viscous protein solution. The progress of the reaction was monitored by tracking the 960 nm NIR feature using an HP Agilent 8453 UV/Vis spectrophotometer and was complete within approximately 1 minute. The sample was subsequently flash frozen again in liquid nitrogen.

S.1.3 Mössbauer spectroscopy. ^{57}Fe Mössbauer spectra were recorded with two spectrometers using Janis Research dewars (4.2 to 200 K) operating in a constant acceleration mode in a transmission geometry. One spectrometer allowed rotation of a small magnet (50 mT) at orientations perpendicular and parallel to the incident gamma radiation. The other contained a superconducting magnet capable of fields up to 7 T aligned parallel to the incident gamma radiation. Isomer shifts were reported relative to Fe metal at 298 K. The simulations of the Mössbauer spectra were performed with least squares fitting using the program SpinCount written by one of the authors.[3] The program uses the standard spin Hamiltonian:

$$H = \beta_e \mathbf{B}\cdot\mathbf{g}\cdot\hat{\mathbf{S}} + \mathrm{D}[\hat{\mathrm{S}}_z^2 - \mathrm{S}(\mathrm{S}+1)/3 + \mathrm{E/D}(\hat{\mathrm{S}}_x^2 + \hat{\mathrm{S}}_x^2)] + \hat{\mathbf{S}}\cdot\mathbf{A}\cdot\hat{\mathbf{I}} - \mathrm{g}_n\beta_n\mathbf{B}\cdot\hat{\mathbf{I}} + (\mathrm{eQV}_{zz}/12)[3\hat{\mathrm{I}}_z^2 - \mathrm{I}(\mathrm{I}+1) + \eta(\hat{\mathrm{I}}_x^2 - \hat{\mathrm{I}}_y^2)]$$

The programs allows for constraints in these variables by performing simultaneous fitting of spectra recorded at multiple applied magnetic fields and variable temperatures.

S.1.4 DFT calculations. The DFT calculations for models for the peroxidatic and His/Tyr heme sites of BthA in both the di-Fe^{3+} and di-Fe^{4+} states were performed with the program suite Gaussian '09 using the pure density functional BP86.[4] For some specified cases, the hybrid density functional B3LYP and user defined functionals obtained from B3LYP by varying the relative contributions of Hartree-Fock (HF) and Slater exchange (SE) to the exchange functional (denoted B3LYP-x, with x the HFE fraction and 1 – x the SE fraction; x = 0.2 in B3LYP). The triple zeta basis set 6-311G was used, unless mentioned otherwise.

The Fermi contact coupling constants, A^{FC}, for Fe^{4+} species are underestimated by our DFT calculations by a factor of ~0.7 and have not been reported.[5] The geometry optimizations used default convergence settings and OPT = modredundant to impose constraints on the internal coordinates defining the position of the Ph ring relative to the porphyrin ring by fixing bond angle Fe-O_{Tyr}-C_{Tyr} and dihedral Fe-O_{Tyr}-C_{Tyr}-C_{Tyr} (these angles are marked in Figure 2, left structure). In unconstrained geometry optimizations these internal coordinates were found to deviate significantly from those in the X-ray structure, available only for the diferric form (see Results and Discussion). Also performed were optimizations in which the Fe-O_{Tyr} bond length in the His/Tyr heme was elongated relative to its optimized value. The DFT solutions for the Fe^{4+} state of the Tyr heme were tested for emerging low-/intermediate-spin Fe^{3+} character and

attendant radical formation on the Ph or porphyrin moieties, using Mulliken spin populations and spin density plots generated by the visualization software GaussView. These analyses showed that the choice of functional had a significant effect on the electronic state calculated for the oxidized His/Tyr heme. As BP86 gave for the His/Tyr heme the best agreement with experiment, all the listed results in this work use BP86 unless specifically stated otherwise.

In the DFT analysis of the S = 1 His/Tyr heme of BthA, three spin states were encountered: (*i*) an S = 1 Fe^{4+} state, (*ii*) an S = 1 spin-coupled low-spin Fe^{3+}–ligand (L) radical state with spin state $|(S_{Fe} = ½, S_L = ½)\ S = 1\rangle$, and (*iii*) an S = 1 spin-coupled intermediate-spin Fe^{3+}–ligand radical state with spin state $|(S_{Fe} = 3/2, S_L = ½)\ S = 1\rangle$. The DFT calculations give for these states the unpaired electron configurations $(\uparrow\uparrow)_{Fe}$ for (*i*), $(\uparrow)_{Fe}(\uparrow)_L$ for (*ii*), and $(\uparrow\uparrow\uparrow)_{Fe}(\downarrow)_L$ for (*iii*) with 2, 1, and 3 unpaired electrons on iron, respectively. The DFT configuration for (*iii*) is the broken symmetry approximation for the S = 1 state. The spin-dipolar contribution to the magnetic hyperfine parameters are printed by Gaussian in the convention $\hat{\boldsymbol{I}} \cdot A^{SD}_{dft} \cdot \hat{\boldsymbol{S}}$ with S = ½ and *I* the nuclear spin of ^{57}Fe. The corresponding A^{SD}_{Fe} values for the Hamiltonian $\hat{\boldsymbol{I}} \cdot A^{SD}_{Fe} \cdot \hat{\boldsymbol{S}}$ with $S = S_{Fe}$ is then obtained by dividing A^{SD}_{dft} by the number of unpaired electrons on iron, that is, by 2 for (*i*), by 1 for (*ii*), and by 3 for (*iii*). To obtain the coupling A^{SD} in the Hamiltonian used for the spectroscopic analysis, $\hat{\boldsymbol{I}} \cdot A^{\mathrm{SD}} \cdot \hat{\boldsymbol{S}}$, where S = 1 is the coupled spin of the metal–ligand system, one has to apply to A^{SD}_{Fe} the familiar spin-projection factors, 1 for (*i*), ½ for (*ii*), and 5/4 for (*iii*). Taken together, these factors yield the expressions $A^{\mathrm{SD}} = A^{SD}_{dft}/2$ for (*i*), $A^{\mathrm{SD}} = A^{SD}_{dft}/2$ for (*ii*), and $A^{\mathrm{SD}} = 5A^{SD}_{dft}/12$ for (*iii*). The A^{SD} values listed in Tables 3 and 5 belong to case (*i*), and the values listed from left to right in Figure 5 belong to case (*i*), (*ii*), and (*iii*), respectively. The isomer shifts calculated with BP86/6-311G were calibrated using a training set of Fe^{3+}, Fe^{4+}, and Fe^{5+} complexes supported by macrocyclic equatorial ligands and oxido, chloride, water, or acetonitrile as axial ligands.[6]

S.2 How to increase δ without changing A^{SD} and A^{FC}?

S.2.1 Electronic considerations. As the iron in the His-Fe^{4+}-Tyr heme is less protected against reduction by the ligands than in His-Fe^{4+}=O heme, one expects a greater admixture of the $\uparrow_{Fe}\uparrow_{Fe}(\uparrow\downarrow)_L$ ground configuration with ligand-to-metal charge transfer configurations, $\uparrow_{Fe}(\uparrow\downarrow)_{Fe}\uparrow_L$ or $(\uparrow\uparrow\uparrow)_{Fe}\downarrow_L$ where ligand L is the porphyrin (P) or Tyr. Equal transfers into d_{xz} or d_{yz} would raise δ while retaining the axiality. The same is true for transfers into d_{z2} and d_{x2-y2}. As the transfer of a full electron raises δ to ~ 0.26 mm/s (Figure 5, middle), the increase of δ from the Fe^{IV}=O value of 0.08 mm/s to 0.17 mm/s would require a ~ 50% admixture of low spin Fe^{3+} and concomitantly lower $\mathbf{A}^{SD}$ and A^{FC} to ~ 0.5 times the values of these parameters for the His/O site. Although a reduction of A^{FC}, albeit a less drastic one, is compatible with experiment, the drop in A^{SD} is clearly at odds with the data.

S.2.2 Effect of the exchange functional on the isomer shift. In the main text it was shown that BP86 gives for the oxidized Tyr-heme an Fe^{4+} ground state with ΔE_Q and A_z^{SD} values in agreement with experiment but a δ that is 0.10 mm/s below the experimental target. In contrast B3LYP gives the $(Fe^{3+}Tyr^{\bullet})_{AF}$ state (Figure 5, right) with ΔE_Q and A_z^{SD} values with the correct sign but a δ (and A_z^{SD}) value that is significantly larger than observed experimentally. These results suggest that δ can be raised by a quantum mechanical admixture of the Fe^{4+} ground state with the $(Fe^{3+}$-$Tyr^{\bullet})_{AF}$ excited state. Interpolation, using the δ values of Figure 5, shows that an admixture of 35% is required to increase δ from 0.08 mm/s to 0.17 mm/s; concomitantly, A_z^{SD} would increase from 13 T (Figure 5, left) to 15 T, slightly exceeding the experimentally

allowed upper limit for this parameter. The mixing of the Fe^{4+} and $(Fe^{3+}Tyr^{\bullet})_{AF}$ configurations (Figure 5, left and right) can be described by DFT as a partial delocalization of the α spin electron from the redox active tyrosine π orbital into one of the vacant 3d orbitals of iron. An obvious cause for the difference between the BP86 and B3LYP results for the oxidized Tyr-heme is in the definition of the exchange term as a pure functional (0% HFE) in BP86 and a hybrid functional (20% HFE) in B3LYP. Conceivably, by making an adjustment to the HFE percentage, a specific quantum mechanical admixture could be obtained that reproduces δ, ΔE_Q, and A_z^{SD} simultaneously within the experimentally allowed margins. To perform this analysis, we employed the user defined functional provided by Gaussian. Starting with BP86 (0% HFE), the HFE was step wise increased to the B3LYP value of 20%, thereby lowering the energy of the $(Fe^{3+}\text{-}Tyr^{\bullet})_{AF}$ state relative to the Fe^{4+} state. Table S1 shows the results of this analysis, including δ values for selected functionals for which we recalibrated the relationship between δ and the electron density at the iron nucleus. The table reveals a jump in both the Fe-O_{Tyr} distance and $\langle \mathbf{S}^2 \rangle_{DFT}$ for B3LYP-0.125, signaling a change in the character of the ground state from Fe^{4+} to $(Fe^{3+}\text{-}Tyr^{\bullet})_{AF}$. The sudden bond length increase reflects both the lowering of the iron valency and the oxidation of the tyrosine, making it a weaker ligand. While the increase in HFE has barely changed δ for B3LYP-0.11, A_z^{SD} has already attained a value incompatible with experiment. The behavior of the DFT results in Table S1 has been explained in Figure S1, which shows a schematic representation of the potential energy surfaces (PES) of the two (weakly) interacting states along the Fe-O_{Tyr} coordinate with minima at 1.84 Å (Fe^{4+}) and 2.25 Å ($(Fe^{3+}\text{-}Tyr^{\bullet})_{AF}$). The double well nature displayed in Figure S1 is supported by B3LYP calculations, which allowed us to secure a local minimum for the Fe^{4+} state with an energy that is 3200 cm^{-1} higher than the global minimum for the $(Fe^{3+}\text{-}Tyr^{\bullet})_{AF}$ ground state for this functional. The admixture of $(Fe^{3+}\text{-}Tyr^{\bullet})_{AF}$ into the Fe^{4+} ground state is inversely proportional to the vertical energy separation between the two states at the ground state minimum (blue vertical lines in Figure S1). The admixture into the Fe^{4+} ground state can be increased by lowering the PES for the $(Fe^{3+}\text{-}Tyr^{\bullet})_{AF}$ state up to the point that the latter state becomes the ground state. The middle diagram of Figure S1 shows the transition point where the admixture of $(Fe^{3+}\text{-}Tyr^{\bullet})_{AF}$ into the Fe^{4+} *ground* state reaches its maximum. The right diagram shows the situation where the two mixing states are degenerate and fully admixed at the minimum for the Fe^{4+} state but now the $(Fe^{3+}\text{-}Tyr^{\bullet})_{AF}$ state is ground state, which was shown to be incompatible with experiment. This analysis shows that increasing δ to 0.17 mm/s with approximate retention of the A_z^{SD} and ΔE_Q values for the Fe^{4+} state is unachievable by engineering the exchange functional. Figure S1 also applies to admixtures with other electron transfers, such as from the porphyrin to the iron ($(Fe^{3+}\text{-}P^{\bullet})_F$, middle diagram of Figure 5 with Tyr radical replaced by a porphyrin radical) and the purported charge resonance between the His/Tyr heme and the tryptophan that intervenes the two heme sites in MauG, which was assigned to the intense absorption band at 960 nm in the electronic absorption spectrum of the oxidized state of MauG.[7] (N.B. Excitation to the $(Fe^{3+}\text{-}Tyr^{\bullet})_{F/AF}$ states provides an alternative interpretation for the 960 nm band, which is consistent with the observation that neither the energy nor the intensity of the 960 nm band change when the intervening tryptophan is replaced by serine or alanine in BthA.[2])

Table S1. Dependence of DFT results for oxidized form of the Tyr heme of BthA on exchange functional[a]

functional	State [b]	$\langle \mathbf{S}^2 \rangle_{DFT}$ [c]	Fe-O_{Tyr} Å	δ [d] mm/s	ΔE_Q mm/s	A_x^{SD} T	A_y^{SD} T	A_z^{SD} T
BP86 [e]	*i*	2.02	1.85	0.10	+2.52	-5.8	-7.5	13.3
B3LYP-0.00	*i*	2.02	1.85	0.11	2.54	-5.6	-7.7	13.3
B3LYP-0.05	*i*	2.03	1.84	–	+2.67	-6.6	-7.7	14.3
B3LYP-0.10	*i*	2.08	1.85	–	+2.78	-8.4	-8.4	16.8
B3LYP-0.11	*i*	2.11	1.86	0.11	+2.78	-8.7	-8.7	17.4
B3LYP-0.125	*iii*	2.58	2.02	–	+2.82	-10.0	-10.2	20.4
B3LYP-0.14	*iii*	2.76	2.11	–	+2.87	-11.0	-11.2	22.2
B3LYP-0.15	*iii*	2.82	2.25	0.33	+2.89	-11.2	-11.5	22.5
B3LYP-0.185	*iii*	2.92	2.23	0.37	+2.97	-11.7	-11.8	23.4
B3LYP [f]	*iii*	2.95	2.25	0.33	+3.03	-11.7	-11.7	23.4
exp			n.d.	0.17	+2.55	-5.3	-5.5	10.8

[a] Im/Tyr model of Figure 2 with constraints on the Fe-O_{Tyr}-C_{Tyr} bond angle and the Fe-O_{Tyr}-C_{Tyr}-C_{Tyr} dihedral given in section S.1.4.

[b] $|S = S_{Fe} = 1\rangle$ (*i*); $|(S_{Fe} = 3/2, S_{Tyr} = ½)\ S = 1\rangle$ (*iii*).

[c] In the ideal case, the expectation value for (*i*) is 2 and for the BS configuration $|M_{Fe} = 3/2, M_{Tyr} = -½\rangle$ (*iii*) is 3.

[d] Cases for which no δ calibration has been determined are indicated by –.

[e] x = 0 for BP86.

[f] B3LYP = B3LYP-0.20.

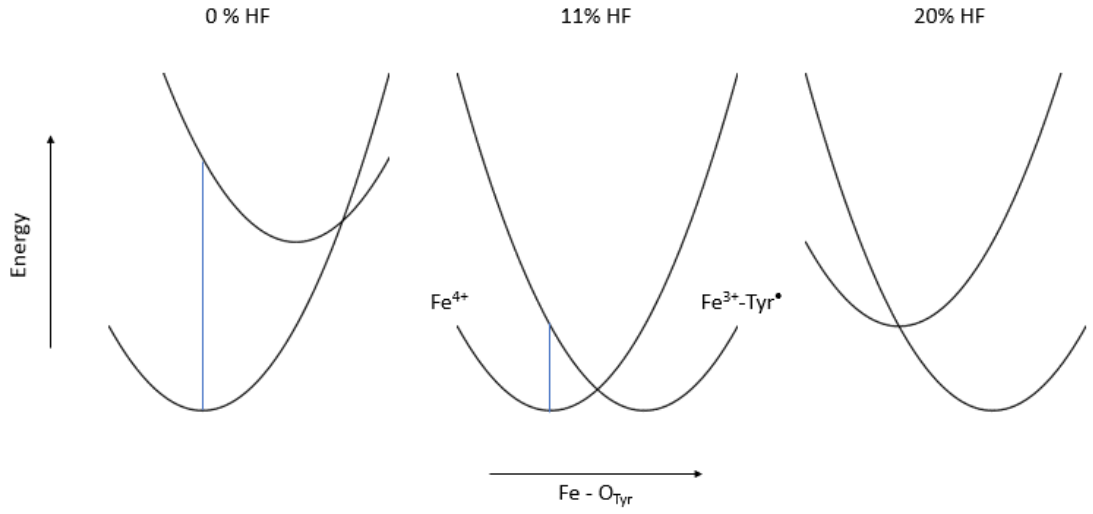

Figure S1. Schematic representation of the potential energy surfaces for the S = 1 Fe^{4+} and $(Fe^{3+}\text{-}Tyr^{\bullet})_{AF}$ states along the Fe – O_{Tyr} distance coordinate as a function of the percent contribution of HFE to the density functional.

S.2.3 Alternative mechanisms. The discussion of Figure S1 showed that δ could not be sufficiently raised either by admixing the S = 1 Fe^{4+} ground configuration with the ligand-to-metal transfer (LTM) state $|(S_{Fe} = 3/2, S_L = ½) S = 1\rangle$ (L = Tyr), hereafter referred to as LTM1, without changing the ground state or increasing A_z^{SD} to a value incompatible with experiment. The spin of the transferred electron in LMT1 is coupled to the S = 1 spin of the Fe^{4+} to give a Hund rule obeying S_{Fe} = 3/2 state. Alternately, one could also consider the admixture with an electronic configuration in which the spin of the transferred electron remains coupled to the unpaired ligand electron as in $\uparrow_{Fe}\uparrow_{Fe}(\uparrow_{Fe}\downarrow_L - \downarrow_L\uparrow_{Fe})/\sqrt{2}$, denoted LTM2. Admixture of LTM2 into the ground state raises δ but leaves the magnetic hyperfine parameters unchanged because the spin of the transferred electron is paired off with the ligand electron. However, LTM2 is a linear combination of the Hund configuration shown in the right diagram of Figure 5 and a non-Hund configuration obtained by flipping the spin of the upper iron electron and is, consequently, higher in energy than LTM1 (*intra*atomic exchange outweighs *inter*atomic exchange). Hence, as shown for LTM1 in the discussion relating to Figure S1, admixture LTM2 is unlikely to be effective in raising δ either.

S.2.4 Influence of Tyr position on δ.

S.2.4.1 Angular dependencies. Having exhausted electronic explanations for the high value for δ in Tyr-heme, we now consider alternative factors affecting this parameter. A structural factor that may affect the isomer shift is the position of the tyrosine relative to the heme moiety and changes therein imposed by the protein environment. The results of a DFT analysis of this factor have been summarized in Table S2. The position of the tyrosine relative to the heme is defined by the bond distance Fe-O_{Tyr} (column 2), the bond angle Fe-O_{Tyr}-C_{Tyr} (column 3), and the dihedral angle Fe-O_{Tyr}-C_{Tyr}-C_{Tyr} (column 4). Unconstrained geometry optimization (row 1) gives a large bond angle (145°) and a short bond distance (1.81 Å) with the tyrosine plane perpendicular to the heme plane (dihedral ~ 0). As noted earlier, the hyperfine parameters (columns 5-8) agree well with experiment, except for δ. Row 2 shows the DFT results for the structure which was optimized with the bond angle and dihedral being constrained to their values in the XRD structure, reported for the diferric state of BthA.[2] The bond angle in the XRD structure (120°) is 25° smaller than obtained in the unconstrained optimization of the Im-Heme-Tyr fragment, the angle between the heme and tyrosine planes has changed to about −90°, minimizing the steric interactions between the two moieties, and the bond length has increased to 1.85 Å. This distance is slightly lower than the bond lengths for low-spin Fe^{3+} from EXAFS of MauG (1.89 Å) and the DFT Im/Ph structure optimized in the low-spin Fe^{3+} state (1.91 Å, Table 3). The Fe-O distances show only modest changes depending on oxidation and spin state. For example, the XRD structures of high-spin Fe^{3+} phenolate complexes have distances of 1.83 Å and 1.85 Å[8, 9] and the angularly constrained DFT structure for the S = 1 Fe^{4+} Im/Ph heme has a bond distance of 1.84 Å (Table 5). The energy of the crystallographically-constrained structure is 1642 cm^{-1} higher than for the unconstrained structure (see column 5), indicating that the protein matrix has a major influence on both structure and energy of the His/Tyr heme site. Meanwhile, the hyperfine parameters, including δ (column 6), have changed little. Row 3 shows that when only the dihedral is constrained, both the bond length and bond angle revert to the values in row 1 and with an energy that is only marginally higher (213 cm^{-1}) than for the unconstrained structure. The latter result shows that the largest contribution to the ΔE value given in row 2 originates mainly from the imposed bond angle change. By

imposing a smaller bond angle (row 4) the steric interaction between the heme and tyrosine moieties becomes noticeable, enforcing a dihedral of $\sim \pm 90°$. The angular constraints considered had little effect on the value for δ.

Table S2. DFT[a] results for the dependence of the hyperfine parameters on the internal coordinates defining the position of the tyrosine relative to the Fe^{4+} heme[b]

Row	Fe – O_{Tyr} (Å)	∠Fe-O_{Tyr}-C_{Tyr} (°)	∠ Fe-O_{Tyr}-C_{Tyr}-C_{Tyr} (°)	ΔE (cm^{-1})	δ (mm/s)	ΔE_Q (mm/s)	$\mathbf{A}^{SD}$ (T)
1	1.81	145	-13	0	0.08	+2.70	-3, -8, +11
2	1.85	***120***[c]	***-95***	1642	0.09	+2.58	-6, -7, +13
3	1.80	141	***-95***	213	0.09	+2.54	-5, -7, +12
4	1.85	***120***	-113	1618	0.08	+2.61	-5, -8, +13
5	***1.91***	142	1	424	0.12	+2.90	-2, -9, +11
6	***1.94***	***120***	***-95***	2095	0.13	+2.82	-6, -7, +13
7	***1.99***	***120***	***-95***	2470	0.15	+2.89	-6, -7, +13
exp	n.d.	n.d.	n.d.	–	0.17	+2.55	-6, -5, +11

[a] BP86/6-311G. [b] Im/Ph structure of Figure 2. [c] Italized bold numbers were fixed during optimization.

S.2.4.2 Distance dependence. We now consider the influence of the Fe-O_{Tyr} distance on the hyperfine parameters (rows 5-7 of Table S2). An increase of the bond length from 1.81 Å (row 1) to 1.91 Å (row 5), followed by reoptimization at fixed bond length, yields a similar bond angle and dihedral as in row 1. The bond lengthening has an energy cost of 424 cm^{-1} and raises δ to 0.12 mm/s, in increment of 0.04 mm/s, without significant changes in the other hyperfine parameters relative to row 1, but still not in agreement with experiment. An increase of 0.09 Å in the bond length of the angularly constrained structure (row 2), followed by reoptimization with fixed values for the bond length, bond angle and dihedral (row 6), increases the energy by 453 cm^{-1} relative to row 2 and raises δ to 0.13 mm/s , again without major alterations in the other hyperfine parameters. A similar calculation, but now for a bond length of 1.99 Å adds 828 cm^{-1} to the energy (compare rows 7 and 2) and increases δ to 0.15 mm/s, close to the experimental target. The energies required for these bond stretches (423 – 828 cm^{-1}) may seem large but are only a fraction (25% - 50 %) of the strain energy associated with the angular distortions imposed by the protein on the His-heme-Tyr moiety (row 2). Table S2 shows that the Fe-O_{Tyr} bond length increases by imposing smaller Fe-O_{Tyr}-C_{Tyr} bond angles but without significantly changing δ. The insensitivity of δ may be the result of a cancelation of the effects on this parameter from the reductions in the donations into the 3d shell due to the angular change (lowering δ) and into the 4s orbital due to the bond length increase (raising δ). In contrast, if the bond length is increased without angular change (rows 5-7) the isomer shift increases. Geometry optimization of the His/Tyr heme in the low-spin ferric state gives a bond angle of 128°, showing that this unit remains strained even in the oxidation state for which the XRD structure (120°) was determined but now with a lower strain energy of 243 cm^{-1} and angular deviation of only 8°. The oxidation of the His/Tyr heme to the Fe^{4+} state raises the strain and angular deviation (25°) sharply and suggests the possibility that there takes place a structural relaxation to mitigate the strain. In this process, the bond length may have acquired a higher value, accounting for the increase in δ.

References

1 E. Arslan, H. Schulz, R. Zufferey, P. Kunzler and L. Thony-Meyer, *Biochem. Biophys. Res. Commun.*, 1998, **251**, 744-747.

2 K. Rizzolo, S. E. Cohen, A. C. Weitz, M. M. Lopez Munoz, M. P. Hendrich, C. L. Drennan and S. J. Elliott, *Nat Commun*, 2019, **10**, 1101.

3 D. T. Petasis and M. P. Hendrich, *Methods Enzymol.*, 2015, **563**, 171-208.

4 Gaussian: Gaussian 09, Revision A.02, M. J. Frisch, G. W. Trucks, H. B. Schlegel, G. E. Scuseria, M. A. Robb, J. R. Cheeseman, G. Scalmani, V. Barone, B. Mennucci, G. A. Petersson, H. Nakatsuji, M. Caricato, X. Li, H. P. Hratchian, A. F. Izmaylov, J. Bloino, G. Zheng, J. L. Sonnenberg, M. Hada, M. Ehara, K.Toyota, R. Fukuda, J. Hasegawa, M. Ishida, T. NakaJima, Y. Honda, O. Kitao, H. Nakai, T. Vreven, J. A. Montgomery, Jr., J. E. Peralta, F. Ogliaro, M. Bearpark, J. J. Heyd, E. Brothers, K. N. Kudin, V. N. Staroverov, R. Kobayashi, J. Normand, K. Raghavachari, A. Rendell, J. C. Burant, S. S. Iyengar, J. Tomasi, M. Cossi, N. Rega, J. M. Millam, M. Klene, J. E. Knox, J. B. Cross, V. Bakken, C. Adamo, J. Jaramillo, R. Gomperts, R. E. Stratmann, O. Yazyev, A. J. Austin, R. Cammi, C. Pomelli, J. W. Ochterski, R. L. Martin, K. Morokuma, V. G. Zakrzewski, G. A. Voth, P. Salvador, J. J. Dannenberg, S. Dapprich, A. D. Daniels, O. Farkas, J. B. Foresman, J. V. Ortiz, J. Cioslowski, and D. J. Fox, Gaussian, Inc., Wallingford CT, 2009.

5 S. Sinnecker, L. D. Slep, E. Bill and F. Neese, *Inorg. Chem.*, 2005, **44**, 2245-2254.

6 V. Vrajmasu, E. Munck and E. L. Bominaar, *Inorg. Chem.*, 2003, **42**, 5974-5988.

7 J. Geng, K. Dornevil, V. L. Davidson and A. Liu, *Proc. Natl. Acad. Sci. U. S. A.*, 2013, **110**, 9639-9644.

8 H. M. Goff, E. T. Shimomura, Y. J. Lee and W. R. Scheidt, *Inorg. Chem.*, 1984, **23**, 315-321.

9 R. H. Heistand, A. L. Roe and L. Que, *Inorg. Chem.*, 1982, **21**, 676-681.